# Kinetic equation and self-organized band formations

Quentin Griette, Sebastien Motsch

April 24, 2018

**Abstract**

Self-organization is an ubiquitous phenomenon in nature which can be observed in a variety of different contexts and scales, with examples ranging from fish schools, swarms of birds or locusts, to flocks of bacteria. The observation of such global patterns can often be reproduced in models based on simple interactions between neighboring particles. In this paper we focus on particular interaction dynamics closely related to the one described in the seminal paper of Vicsek and collaborators. After reviewing the current state of the art in the subject, we study a numerical scheme for the Vicsek and Frouvelle-Liu kinetic equations of interacting particles, which has the specificity of preserving many physical properties of the continuous models, like the positivity and the entropy. We describe a stable pattern of bands emerging in the Frouvelle-Liu dynamics and give some insights about the relationship between their formation, the mean density and the strength of the ambient noise.

## Contents

# 1 Introduction

Swarming dynamics have attracted a lot attention in recent years raising the question how simple interaction rules could lead to complex pattern formation [22]. One of the main difficulty is to link the individual behaviors of agents and the pattern formations observed at a larger scale. Fortunately the framework of kinetic equations allows such transition between micro and macro dynamics. Among the many swarming models introduced [3], the Vicsek model [21] is one of the most popular since it is a rather simple dynamics (there is only alignment) with few parameters but it is however able to generate complex pattern which are challenging to predict analytically. The Vicsek model have been well studied both numerically [6,18,19] or analytically [2,12,16] and the derivation of its kinetic and macroscopic equation is well-understood [9,10]. However, as noted first by Chaté and Grégoire [18], there exists a certain regime where the Vicsek model leads to the formation of traveling bands. Many numerical studies have been conducted to better analyze the formation of these bands at the particle level but no work has been proposed to study the bands using kinetic or macroscopic framework. This manuscript aims at to proposing a first study on such band formation from the angle of kinetic equation.

After the discovery of band formation in the Vicsek dynamics by Chaté and Grégoire [18], there has been a debate [1, 5] about the order of the phase transition in the Vicsek model (continuous or discontinuous). As there was no analytic framework available, the conjecture could be only based on (particle) numerical simulation. However, the derivation of kinetic and macroscopic equation for the Vicsek model [9,10] indicated that in a dense regime of particles (the so-called moderately interacting particle [20]), the Vicsek model has a continuous transition from order to disorder. In this regime of high density, no phase transition or band formation could be observed. A major discovery was then provided by Frouvelle and Liu [7, 8, 14] were a modification of the (continuum) Vicsek was considered: alignment is proportional to the density. In their dynamics, a phase transition occurs: at low density, the velocity distribution becomes uniform, whereas at large density, the dynamics converge to a so-called von Mises distribution. This analytic result was only proven in an homogeneous setting (no spatial variable). Thus, it is still unknown what effect would have a transport term on the dynamics. This is however a very challenging question as the transport term breaks the entropy dissipation. In this manuscript, we propose to investigate numerically the Frouvelle-Liu dynamics in a non-homogeneous setting.

Starting from the kinetic equation associated with the Vicsek model, we first review some properties of the collisional operator (entropy dissipation) that will be central for the building of our numerical scheme. Most of the estimate are built on the Fokker-Planck structure of the operator. We do take advantage of this formulation in the design of our numerical scheme. The key properties of the collision operator (positivity preserving, entropy dissipation) are also satisfied for the discrete operator. Since we aim at analyzing the long-time behavior of the solution, it is essential to preserve these properties. For instance, several papers have already proposed to solve numerically the kinetic equation associated with the Vicsek model using other methods (spectral method [15], particle method [11], discontinuous Galerkin [13]). But we rather have lower accuracy and a preserving numerical scheme to study the long-time behavior of the solution (even though our scheme is still second order accurate in the velocity-variable). We then explore the dynamics of the kinetic equation in various regimes. In the original Vicsek model, no band formations are observed, the spatial density becomes

homogeneous while the velocity distribution become distributed according to a (global) von Mises distribution. In the Frouvelle-Liu dynamics however, when the density is above a threshold, band formation occurs starting from random initial configuration. As far as the authors know, this is the first time such band formations are observed at the kinetic level. Band were also observed in [13] but there were only 'transient', the density profile would become flat after a long time. Here, the density profile is not flattening out, but instead is becoming more and more concentrated. Numerically, we have to introduce an adaptive time step to deal with a demanding CFL condition.

Although our numerical investigation suggest that band formation emerge from the Frouvelle-Liu dynamics, it would be crucial to also develop an analytic framework to further understand. Our result indicate that the transport operator could further the alignment operator making concentration. From these observations, it seems unlikely that there exists an analytic profile for these band formations. But the question remains open. Similar, we could perform simulation in dimension 3, but the discretization of the unit sphere $\mathbb{S}^2$ is more delicate than $\mathbb{S}^1$ (there is no 'uniform grid' on $\mathbb{S}^2$) and thus having discrete entropy dissipation or symmetry preserving would be more challenging. Finally, higher order accuracy in time discretization should also be investigating using for instance [4, 17].

# 2 Microscopic description

## 2.1 Vicsek model

The Vicsek model [10, 21] at the particle level describe the motion of $N$ particles with position $\mathbf{x}_i \in \mathbb{R}^d$ (with $d = 2, 3$) and a direction $\omega_i \in \mathbb{S}^{d-1}$ (i.e. $|\omega_i| = 1$). The evolution of the particles is given by the following system:

$$\begin{aligned} \mathbf{x}_i' &= c\omega_i \\ \mathrm{d}\omega_i &= P_{\omega_i^\perp}(\mu\,\Omega_i \mathrm{d}t + \sqrt{2\sigma} \circ \mathrm{d}B_i^t), \end{aligned} \tag{2.1}$$

where $c > 0$ is the speed of the particle, $\mu$ is the strength of the alignment interaction, $\sigma$ is the intensity of the noise and $\mathrm{d}B_i^t$ are independent white noise, $P_{\omega_i^\perp}$ is the orthogonal projection on the orthogonal of $\omega_i$

$$P_{\omega_i^\perp} = \mathrm{Id} - \omega_i \otimes \omega_i \tag{2.2}$$

it ensures that $|\omega_i(t)| = 1$ over time, $\Omega_i$ is the average direction of the particle $i$:

$$\Omega_i = \frac{\mathbf{j}_i}{|\mathbf{j}_i|}\,, \quad \mathbf{j}_i = \sum_{j, |\mathbf{x}_j - \mathbf{x}_i| \le R} \omega_j, \tag{2.3}$$

with $R$ the radius of interaction,

## 2.2 Frouvelle-Liu dynamics

Frouvelle and Liu [8, 14] proposed a modification of the dynamics where the alignment interaction $\mu$ is proportional to the norm of the flux $\mathbf{j}_i$:

$$\begin{aligned} \mathbf{x}_i' &= c\omega_i \\ \mathrm{d}\omega_i &= P_{\omega_i^\perp}(\mu\,\mathbf{j}_i \mathrm{d}t + \sqrt{2\sigma} \circ \mathrm{d}B_i^t). \end{aligned} \tag{2.4}$$

This modification has several consequences: i) the Vicsek model 2.1 is not-defined when the flux $\mathbf{j}_i$ equal zero ($\Omega_i$ not defined) where the Frouvelle-Liu dynamics does not have any singularity, ii) there is a phase transition in the dynamics (2.4) as the number of particles increases (or similarly as $\mu$ increases). The kinetic description of this dynamics will allow to better explain this phase transition (see section 3.2).

## 2.3 Band formation

Band formations have been first analyzed by Grégoire and Chaté [18] in the case of the original *discreet* Vicsek model and several numerical studies have been conducted since [1, 6, 19]. To motivate our study, we present numerically an example of such band formation in the context of the *continuous* dynamics (2.1).

The numerical simulation is performed with $N = 30,000$ particles on a square domain with length $L = 4$ and periodic boundary condition. Initially, particles are distributed at random in space and velocity. Table 1 gives the list of values for the parameters. We observe in figure 1 the formation of a traveling wave moving in the $x$-direction. To further quantity this formation, we estimate the average density $\rho$ and velocity $u$ in the $x$-direction:

$$\rho(x,t) = \#\{i : x - \Delta x/2 \leq x_i(t) \leq x + \Delta x/2\} \tag{2.5}$$

$$\rho(x,t)u(x,t) = \sum_{i:\, x-\Delta x/2 \leq x_i(t) \leq x+\Delta x/2} \cos\theta_i. \tag{2.6}$$

where $x_i$ and $\cos\theta_i$ are resp. the $x$-component of the position vector $\mathbf{x}_i$ and velocity $\omega_i$. We give an example of such $\rho$ and $u$ in the figure 2.

We notice that the regime in which the band formation occur is far from being dense. Indeed, in a homogeneous setting, the average number of neighbors is given by:

$$\text{Average neighbors} \approx \frac{|B(0,R)|}{L^2} \times N = 2.36,$$

therefore we are far from being in kinetic regime (let alone macroscopic region). Thus, the validity of the kinetic equation associated with the dynamics (described in the next section) is questionable in this regime. Particles are not necessarily 'moderately interacting' [20].

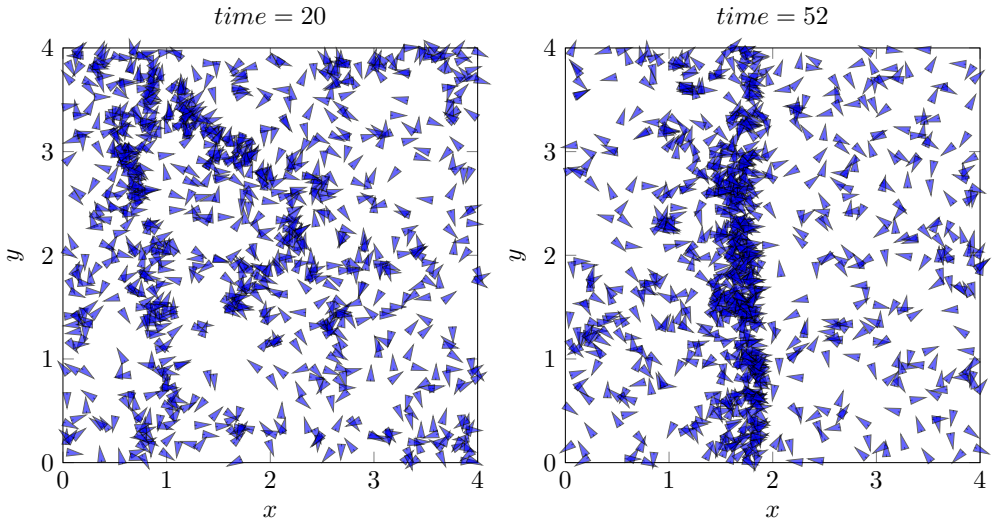


Figure 1: Illustration of the simulation of the Vicsek model (2.1) at two different time. We observe the formation of a vertical *band*. See table 1 for the parameters used.

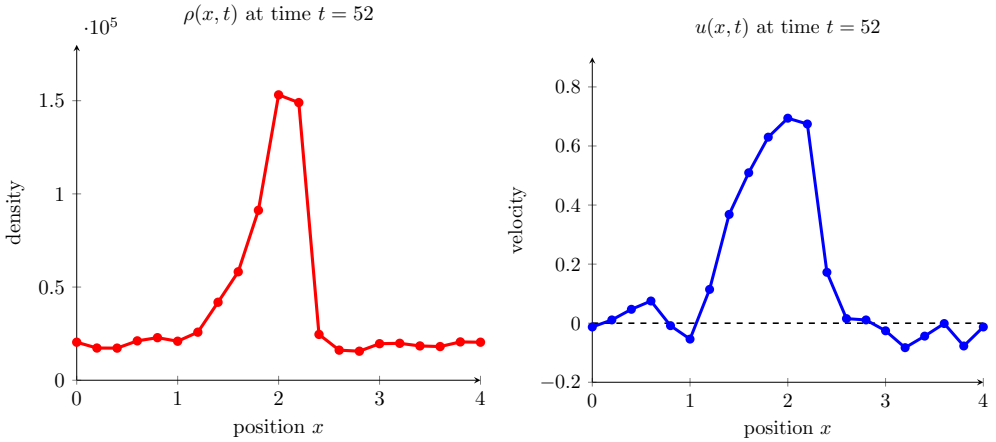


Figure 2: Density $\rho$ and average velocity $u$ in the $x$-direction at $t = 52$. Where the density $\rho$ is larger, the speed $u$ increases.

| Description | notation | value |
|---|---|---|
| Number particles | $N$ | $30,000$ |
| Strength alignment | $\mu$ | 100 |
| Noise intensity | $\sigma$ | 20 |
| Radius interaction | $R$ | .02 |
| Length domain | $L$ | 4 |
| Time step | $\Delta$t | $10^{-2}$ |

Table 1: Parameters used in the simulations for figures 1-2

# 3 Kinetic description

## 3.1 Introduction

The kinetic equation associated with the Vicsek dynamics (2.1) is described through the density distribution $f(\mathbf{x}, \omega, t)$. As the number of particles $N$ tends to infinity, the particle dynamics converge to the solution of a deterministic equation given by [2]

$$\partial_t f + c\,\omega \cdot \nabla_{\mathbf{x}} f = -\mu \nabla_\omega \cdot (P_{\omega^\perp}(\Omega_f)\, f) + \sigma \Delta_\omega f \tag{3.1}$$

where $c > 0$ is the speed of the particles, $\mu > 0$ is the intensity of the relaxation toward the mean velocity and $\sigma > 0$ is the diffusion coefficient and $P_{\omega^\perp}$ the projection operator (2.2), $\Omega$ is the mean velocity at the point $\mathbf{x}$

$$\Omega_f(\mathbf{x}) = \frac{\mathbf{j}_f(\mathbf{x})}{|\mathbf{j}_f(\mathbf{x})|} \quad \text{with} \quad \mathbf{j}_f(\mathbf{x}) = \int_{y \in B(\mathbf{x},R), \omega \in \mathbb{S}^{d-1}} \omega f(\mathbf{y}, \omega)\, \mathrm{d}\mathbf{y}\mathrm{d}\omega, \tag{3.2}$$

$R > 0$ being the radius of interaction.

The Frouvelle-Liu dynamics lead to a similar kinetic equation except for the transport term in $\omega$:

$$\partial_t f + c\,\omega \cdot \nabla_{\mathbf{x}} f = -\mu \nabla_\omega \cdot (P_{\omega^\perp}(\mathbf{j}_f)\, f) + \sigma \Delta_\omega f. \tag{3.3}$$

in other words the strength $\mu$ of alignment is now proportional to $|\mathbf{j}_f|$.

## 3.2 Homogeneous case

To investigate kinetic equations, we study the homogeneous case, assuming that $f$ is independent of $\mathbf{x}$. Thus, the kinetic equations (3.1) and (3.3) become:

$$\partial_t f = Q(f) \tag{3.4}$$

with:

$$Q(f) \quad = \quad -\mu_f \nabla_\omega \cdot (P_{\omega^\perp}(\Omega_f)\, f) + \sigma \Delta_\omega f \tag{3.5}$$

and $\Omega_f = \frac{\mathbf{j}_f}{|\mathbf{j}_f|}$ with $\mathbf{j}_f = \int_{\omega \in \mathbb{S}^{d-1}} \omega f(\omega)\, \mathrm{d}\omega$ and

$$\mu_f = \begin{cases} \mu & \text{Vicsek dynamics} \\ \\ \mu |\mathbf{j}| & \text{Frouvelle-Liu dynamics.} \end{cases} \tag{3.6}$$

The operator $Q$ (3.5) can be written as Fokker-Planck type equation introducing:

$$\phi(\omega) = \begin{cases} \langle \mathbf{j}_f, \omega \rangle & \text{Vicsek dynamics} \\ \\ \langle \Omega_f, \omega \rangle & \text{Frouvelle-Liu dynamics.} \end{cases} \tag{3.7}$$

with $\langle , \rangle$ the usual scalar product in $\mathbb{R}^n$, we find:

$$Q(f) = \sigma \nabla_\omega \cdot \left( M_f \nabla_\omega \cdot \left( \frac{f}{M_f} \right) \right) \quad , \text{ with} \quad M_f(\omega) = \mathrm{e}^{\frac{\mu}{\sigma}\phi(\omega)} \tag{3.8}$$

using the identity $\nabla_\omega \langle \mathbf{u}, \omega \rangle = P_{\omega^\perp}(\mathbf{u})$. We deduce a first identity:

$$\int_\omega \partial_t f \frac{f}{M_f} \, \mathrm{d}\omega = -\sigma \int_\omega M_f \left| \nabla_\omega \left( \frac{f}{M_f} \right) \right|^2 \, \mathrm{d}\omega \leq 0. \tag{3.9}$$

Unfortunately, the left-hand side of (3.9) cannot be written as a total time derivative and thus we cannot deduce any *entropy decay*. The *trick* is to notice the following:

$$\begin{aligned} Q(f) &= \sigma \nabla_\omega \cdot \left( f \frac{M_f}{f} \nabla_\omega \cdot \left( \frac{f}{M_f} \right) \right) & (3.10) \\ &= \sigma \nabla_\omega \cdot \left( f \, \nabla_\omega \cdot \ln \left( \frac{f}{M_f} \right) \right). & (3.11) \end{aligned}$$

Therefore,

$$\int_\omega \partial_t f \, \ln \left( \frac{f}{M_f} \right) \, \mathrm{d}\omega = -\sigma \int_\omega f \left| \nabla_\omega \ln \left( \frac{f}{M_f} \right) \right|^2 \, \mathrm{d}\omega \leq 0. \tag{3.12}$$

Thanks to the property of the logarithm, the left-hand side can now be written as a total time derivative and we deduce the following proposition.

**Proposition 3.1** *Suppose $f$ solution to the homogeneous kinetic equation* (3.4) *and consider the free energy:*

$$\mathcal{F}[f] = \int_\omega f \, \ln f \, \mathrm{d}\omega - \frac{\mu}{\sigma} \Phi_f, \tag{3.13}$$

*with:*

$$\Phi_f = \begin{cases} |\mathbf{j}_f| & \textit{Vicsek dynamics} \\ \frac{1}{2} |\mathbf{j}_f|^2 & \textit{Frouvelle-Liu dynamics.} \end{cases} \tag{3.14}$$

*It satisfies:*

$$\frac{d}{dt} \mathcal{F} = -\sigma \int_\omega f \left| \nabla_\omega \ln \left( \frac{f}{M_f} \right) \right|^2 \, \mathrm{d}\omega \leq 0. \tag{3.15}$$

**Proof.** We only need to show that left-hand side of (3.12) is a total derivative:

$$\begin{aligned} \int_\omega \partial_t f \, \ln \left( \frac{f}{M_f} \right) \, \mathrm{d}\omega &= \int_\omega \partial_t f \, \left( \ln f - \frac{\mu}{\sigma} \phi \right) \, \mathrm{d}\omega & (3.16) \\ &= \int_\omega \partial_t (f \, \ln f) - \frac{\mu}{\sigma} \partial_t f \cdot \phi \, \mathrm{d}\omega & (3.17) \end{aligned}$$

using the conservation of mass $\int_\omega \partial_t f \, \mathrm{d}\omega = 0$. Notice moreover that $\phi$ (3.7) can be expressed as gradient (making the dynamics (3.5) a gradient flow as noted in [12]). Indeed, taking $f + \varepsilon$ a small perturbation of $f$, we have:

$$\begin{aligned} |\mathbf{j}_{f+\varepsilon}|^2 &= \left| \int_\omega (f + \varepsilon) \omega \, \mathrm{d}\omega \right|^2 = |\mathbf{j}_f|^2 \, + \, 2 \langle \int_\omega f \omega \, \mathrm{d}\omega, \int_\omega \varepsilon \omega \, \mathrm{d}\omega \rangle \, + \, \mathcal{O}(\varepsilon^2) & (3.18) \\ &= |\mathbf{j}_f|^2 \, + \, 2 \int_\omega \langle \mathbf{j}_f, \omega \rangle \varepsilon \, \mathrm{d}\omega \, + \, \mathcal{O}(\varepsilon^2), & (3.19) \end{aligned}$$

thus $\frac{\delta |\mathbf{j}_f|^2}{\delta f}(\omega) = 2 \langle \mathbf{j}_f, \omega \rangle$. One deduces $\phi = \frac{\delta \Phi}{\delta f}$ with $\Phi$ given by (3.14). We deduce:

$$\int_\omega \partial_t f \cdot \phi(\omega) \, \mathrm{d}\omega = \int_\omega \partial_t f \cdot \frac{\delta \Phi}{\delta f}(\omega) \, \mathrm{d}\omega = \frac{\mathrm{d}}{\mathrm{d}t} \Phi(f(t)) \tag{3.20}$$

Therefore, we obtain:

$$\int_\omega \partial_t f \, \ln\left(\frac{f}{M_f}\right) \mathrm{d}\omega \quad = \quad \frac{\mathrm{d}}{\mathrm{d}t}\mathcal{F} \tag{3.21}$$

with $\mathcal{F}$ given by (3.13). □

## 3.3 Phase transition

Since the dynamics (3.5) have entropy, one can study the long-time behavior and deduce the convergence toward equilibrium given as the minimizer of the *free energy* $\mathcal{F}$ (3.13). But first we need to identify the minimizers of $\mathcal{F}$. To do so, we notice that once we fix the flux $\mathbf{j}_f$, the minimizer would be given by von Mises.

**Lemma 3.2** *Fix* $\mathbf{j}$ *with* $0 < |\mathbf{j}| < 1$ *and consider the affine space:*

$$\mathcal{A} = \left\{ f \in L^2(\mathbb{S}^{n-1}) \;\middle|\; \int_{\mathbb{S}^{n-1}} \omega f(\omega)\,\mathrm{d}\omega = \mathbf{j} \quad \textit{and} \quad \int_{\mathbb{S}^{n-1}} f(\omega)\,\mathrm{d}\omega = 1 \right\}. \tag{3.22}$$

*Then:*

$$\inf_{\mathcal{A}} \left\{ \int_\omega f \, \ln f \,\mathrm{d}\omega \right\} = \int_\omega M_* \, \ln M_* \,\mathrm{d}\omega \tag{3.23}$$

*with* $M_*$ *von Mises* (3.8) *satisfying* $\int_\omega \omega M_*(\omega)\,\mathrm{d}\omega = \mathbf{j}$.

**Proof.** Assume there exists a minimizer $f_*$ and rewrite the constraint as

$$H[f] = \int f \ln f \;\;, \quad \alpha[f] = \left| \int_{\mathbb{S}^{n-1}} \omega f - \mathbf{j} \right|^2 - 1 \;\;, \quad \beta[f] = \left( \int_{\mathbb{S}^{n-1}} f - 1 \right)^2. \tag{3.24}$$

Denote $\lambda_1$ and $\lambda_2$ the Lagrange multiplier associated with $f_*$:

$$\left.\frac{\delta H}{\delta f}\right|_{f_*} \quad = \quad \lambda_1 \left.\frac{\delta \alpha}{\delta f}\right|_{f_*} + \lambda_2 \left.\frac{\delta \beta}{\delta f}\right|_{f_*} \tag{3.25}$$

$$\Rightarrow \ln f_* + 1 \quad = \quad \lambda_1 \, 2\omega \cdot (-\mathbf{j}) + \lambda_2 \cdot 0. \tag{3.26}$$

since $\int f_* = 1$. Thus, taking the exponential leads to:

$$f_*(\omega) = C \mathrm{e}^{-2\lambda_1 \omega \cdot \mathbf{j}}$$

and therefore $f_*$ is a von Mises distribution. □

As a consequence of the lemma, we can restrict the search of minimizers of the free energy $\mathcal{F}$ on von Mises distributions. In figure 3, we estimate numerically the entropy $\int_\omega M \ln M$ of von Mises distribution depending on their average velocity $|\mathbf{j}| = |\int_\omega \omega M|$ along with its approximation near $\mathbf{j} \approx 0$:

$$\int_\omega M \log M = -\log 2\pi + |\mathbf{j}|^2 \; + \; \mathcal{O}(|\mathbf{j}|^3). \tag{3.27}$$

We deduce that the free energy $\mathcal{F}$ for the Vicsek model will never have a minimum at $\mathbf{j} = 0$ meaning that the uniform distribution is never stable. However, for the Frouvelle-Liu dynamics, when the diffusion $\sigma$ is large, the free entropy $\mathcal{F}$ will be minimum at $\mathbf{j} = 0$ and therefore the uniform distribution will become the stable equilibrium. These two situations are depicted in figure 4.

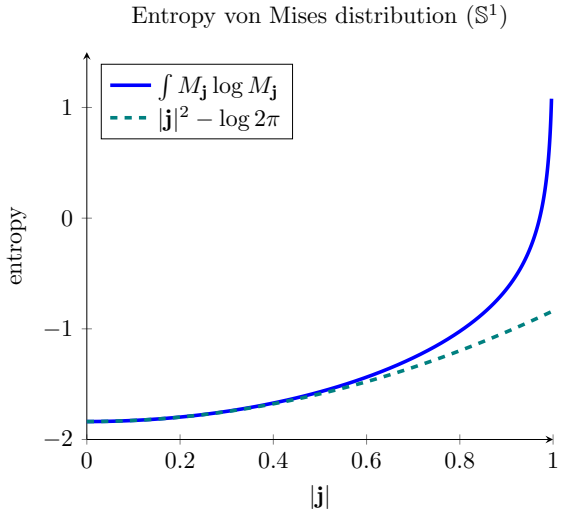


Figure 3: Entropy $\int M \log M$ for $M$ von Mises distribution as a function of the length $|\int \omega M|$. The curve increases quadratically near $|\mathbf{j} = 0$.

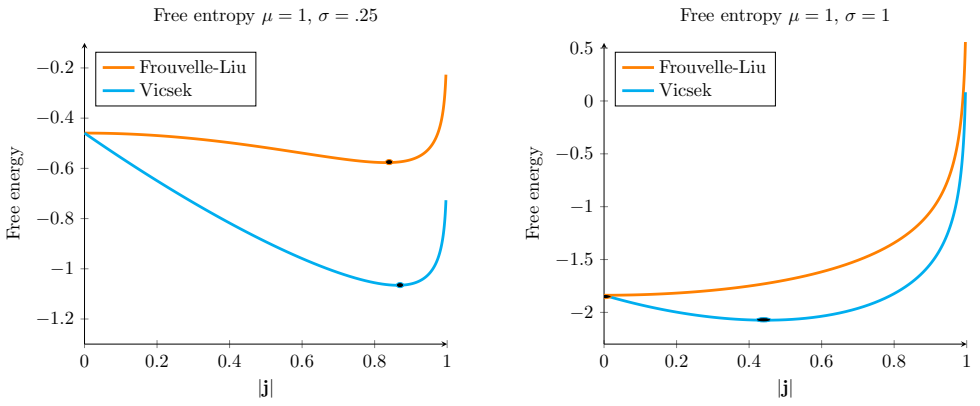


Figure 4: **Left**: for low value of the diffusion coefficient $\sigma$, the minimizers for both free entropy are von Mises distribution. **Right**: when the diffusion coefficient $\sigma$ exceeds a certain threshold, the uniform distribution, i.e. $\mathbf{j} = 0$, becomes the minimizer for the Frouvelle-Liu dynamics.

# 4 Numerical scheme

Several schemes have already been proposed to study the kinetic equation (3.1) using spectral method [15], discontinuous Galerkin [13] or semi-Lagrangian [11]. However, we are now interested in the long time behavior of the solution, thus we would like to design a numerical scheme with several properties:

- conservative, preserve positivity (under some CFL condition)
- satisfy a discrete version of inequalities (3.9) and (3.12)

In the following, we study the 2D scenario taking advantage that the velocity space $\omega \in \mathbb{S}^1$ can be parametrized using polar coordinates by $\theta \in \mathbb{R}/2\pi\mathbb{Z}$ with $\omega = \begin{pmatrix}\cos\theta \\ \sin\theta\end{pmatrix}$. Thus, the kinetic equation (3.1) becomes:

$$\partial_t f + c\,\omega \cdot \nabla_{\mathbf{x}} f = -\mu(f)\,\partial_\theta(\sin(\bar{\theta} - \theta) f) + \sigma \partial_\theta^2 f, \tag{4.1}$$

where $\bar{\theta}$ is such that:

$$\Omega = \begin{pmatrix}\cos\bar{\theta} \\ \sin\bar{\theta}\end{pmatrix} \tag{4.2}$$

and $\mu(f)$ is either a constant (Vicsek model) or proportional to $|\mathbf{j}|$ (Frouvelle-Liu dynamics). Our numerical scheme is then based on a splitting method solving separately:

- the *transport part*
$$\partial_t f + c\,\omega \cdot \nabla_{\mathbf{x}} f = 0 \tag{4.3}$$
- the *collision part* :
$$\partial_t f = Q(f) \tag{4.4}$$
where $Q(f) = -\mu_f \partial_\theta(\sin(\bar{\theta} - \theta) f) + \sigma \partial_\theta^2 f$

## 4.1 Collision operator

In this section we focus on numerically solving equation (4.4). We write:

$$Q(f) = -\mu(f)\partial_\theta(\sin(\bar{\theta} - \theta) f) + \sigma \partial_\theta^2 f = \sigma \partial_\theta \left( M_f \partial_\theta \left( \frac{f}{M_f} \right) \right) \tag{4.5}$$

where $M_{\bar{\theta}}$ is the *Von Mises distribution* :

$$M_f(\theta) = C_0 \exp^{\frac{\mu(f)}{\sigma}\cos(\theta - \bar{\theta})},$$

where $C_0$ is a normalization constant. Here, we simply take $C_0 = 1$.

### 4.1.1 Discretization in $\theta$

Fix $N > 0$ and consider a uniform discretization of the interval $[0, 2\pi)$ with $\theta_k = i\Delta\theta$ and $\Delta\theta = \frac{2\pi}{N}$. Denote: $f_k = f(\theta_k)$ and $f_{k+\frac{1}{2}} = f(\theta_k + \Delta\theta/2)$ and similarly $M_k = M_f(\theta_k)$. To approximate $Q$ (which is a differential operator), we use the second order approximation:

$$\partial_\theta \left( \frac{f}{M_f} \right)\Big|_{\theta_k} = \frac{1}{\Delta\theta} \left( \frac{f_{k+\frac{1}{2}}}{M_{k+\frac{1}{2}}} - \frac{f_{k-\frac{1}{2}}}{M_{k-\frac{1}{2}}} \right) + \mathcal{O}(\Delta\theta^2)$$

which gives

$$Q(f)(\theta_k) = Q_N(f)(\theta_k) + \mathcal{O}(\Delta\theta^2),$$

with

$$\begin{aligned} Q_N(f)(\theta_k) &= \frac{\sigma}{\Delta\theta^2}\left[M_{k+\frac{1}{2}}\left(\frac{f_{k+1}}{M_{k+1}} - \frac{f_i}{M_i}\right) - M_{k-\frac{1}{2}}\left(\frac{f_k}{M_k} - \frac{f_{k-1}}{M_{k-1}}\right)\right] \quad (4.6)\\ &= \frac{\sigma}{\Delta\theta^2}\left[\frac{M_{k+\frac{1}{2}}}{M_{k+1}} f_{k+1} - \left(\frac{M_{k+\frac{1}{2}} + M_{k-\frac{1}{2}}}{M_k}\right) f_k + \frac{M_{k-\frac{1}{2}}}{M_{k-1}} f_{k-1}\right]. \quad (4.7)\end{aligned}$$

The discrete operator $Q_N$ can be identified with a square $N \times N$ matrix:

$$Q_N := \frac{\sigma}{\Delta\theta^2}\begin{pmatrix} b_1 & c_1 & 0 & \cdots & 0 & a_1 \\ a_2 & b_2 & c_2 & \cdots & & 0 \\ 0 & a_3 & b_3 & & & \vdots \\ \vdots & & & \ddots & & \\ 0 & & & & b_{n-1} & c_{n-1} \\ c_n & 0 & \cdots & & a_n & b_n \end{pmatrix} \quad (4.8)$$

and

$$a_k = \frac{M_{k-\frac{1}{2}}}{M_{k-1}}, \quad b_k = -\frac{M_{k+\frac{1}{2}} + M_{k-\frac{1}{2}}}{M_k}, \quad c_k = \frac{M_{k+\frac{1}{2}}}{M_{k+1}} \quad (4.9)$$

with a slight abuse of notation such as $M_{-\frac{1}{2}} = M_{N-\frac{1}{2}}$ (by periodicity of $M$).

The discrete operator $Q_N$ has many features of the differential operator $Q$. Denote the scalar product:

$$\langle u, v\rangle_{M^{-1}} = \sum_{i=1}^{N} \frac{u_k v_k}{M_k},$$

the operator $Q_N$ satisfies some equivalent relation as (3.9) and (3.12).

**Proposition 4.1** *The operator $Q_N$ (4.6) is symmetric with respect to this scalar product:*

$$\langle Q_N(u), v\rangle_{M^{-1}} = \langle u, Q_N(v)\rangle_{M^{-1}}$$

*and satisfies:*

$$\begin{aligned} \langle Q_N(u), u\rangle_{M^{-1}} &= -\frac{\sigma}{\Delta\theta^2}\sum_k M_{k+\frac{1}{2}}\left(\frac{u_{k+1}}{M_{k+1}} - \frac{u_k}{M_k}\right)^2 \le 0 \quad (4.10)\\ \langle Q_N(u), \ln\frac{u}{M}\rangle &\le 0. \quad (4.11)\end{aligned}$$

**Proof.** Take any vectors $u$ and $v$, Abel formula (discrete integration by parts) gives:

$$\begin{aligned} \langle Q_N(u), v\rangle_{M^{-1}} &= \frac{\sigma}{\Delta\theta^2}\sum_k M_{k+\frac{1}{2}}\left(\frac{u_{k+1}}{M_{k+1}} - \frac{u_k}{M_k}\right)\left(\frac{v_k}{M_k} - \frac{v_{k+1}}{M_{k+1}}\right) \quad (4.12)\\ &= \langle u, Q_N(v)\rangle_{M^{-1}}.\end{aligned}$$

From (4.6), we also deduce (4.10).

Moreover, using once again Abel formula:

$$\langle Q_N(u), \ln \frac{u}{M} \rangle = \frac{\sigma}{\Delta\theta^2} \sum_k M_{k+\frac{1}{2}} \left( \frac{u_{k+1}}{M_{k+1}} - \frac{u_k}{M_k} \right) \left( \ln \frac{u_k}{M_k} - \ln \frac{u_{k+1}}{M_{k+1}} \right).$$

Thus, denoting $x = \frac{u_{k+1}}{M_{k+1}}$ and $y = \frac{u_k}{M_k}$, we have an expression of the form:

$$(x-y)(\ln y - \ln x) = (x-y) \ln \frac{y}{x} \leq 0$$

for any $x, y > 0$. We deduce (4.11). □

### 4.1.2 Explicit Euler

The Euler method can be used to discretize in time the collisional part of the kinetic equation (4.4):

$$f^{n+1} = f^n + \Delta t Q_N(f^n) = (\mathrm{Id} + \Delta t Q_N) f^n.$$

A sufficient condition to have $L^\infty$ stability of the scheme is to have the matrix $\mathrm{Id} + \Delta t Q_N$ positive matrix (i.e. all coefficients positive). This sufficient condition leads to the following CFL condition:

$$\max_k \{|b_k|\} \frac{\sigma \Delta t}{\Delta \theta^2} < 1, \tag{4.13}$$

which is usual for diffusion type operator. Moreover, if the CFL condition is met, then positivity and mass are preserved.

**Remark 4.2** *We can find an explicit sufficient condition to guarantee the CFL condition* (4.13)*. Indeed, writing:*

$$\begin{aligned} \frac{M_{k+\frac{1}{2}}}{M_k} &= \frac{\exp\left(\frac{\mu_f}{\sigma} \cos(\theta_{k+\frac{1}{2}} - \overline{\theta})\right)}{\exp\left(\frac{\mu_f}{\sigma} \cos(\theta_k - \overline{\theta})\right)} = \exp\left(\frac{\mu_f}{\sigma} [\cos(\theta_{k+\frac{1}{2}} - \overline{\theta}) - \cos(\theta_k - \overline{\theta})]\right) \\ &= \exp\left(-2\frac{\mu_f}{\sigma} \sin\left(\theta_k - \overline{\theta} + \frac{\Delta\theta}{4}\right) \sin\left(\frac{\Delta\theta}{4}\right)\right) \end{aligned}$$

*using* $\cos\alpha - \cos\beta = -2 \sin\frac{\alpha+\beta}{2} \sin\frac{\alpha-\beta}{2}$*. We deduce*

$$\frac{M_{k+\frac{1}{2}}}{M_k} \leq \exp\left(2\frac{\mu_f}{\sigma} \sin\left(\frac{\Delta\theta}{4}\right)\right).$$

*and find:*

$$\max |b_k| \leq 2 \exp\left(2\frac{\mu_f}{\sigma} \sin\left(\frac{\Delta\theta}{4}\right)\right) = 2 + \frac{\mu_f}{\sigma} \Delta\theta + \mathcal{O}(\Delta\theta^2).$$

*This leads to the tractable (sufficient) CFL condition:*

$$\frac{2\sigma\Delta t}{\Delta\theta^2} < \exp\left(-2\frac{\mu_f}{\sigma} \sin\left(\frac{\Delta\theta}{4}\right)\right). \tag{4.14}$$

**Algorithm 1** Collision part eq. (4.4)

**procedure** COLLISION($f(\theta_k), \Delta t$)
  $\mathbf{j} = \sum_k \omega_k f_k \Delta\theta$; $\overline{\theta} = angle(\mathbf{j})$
  $M_k = \exp(\frac{\mu_f}{\sigma}\cos(\theta_k - \overline{\theta}))$
  **for** $k$ in $1 : N$ **do**
    $Q_N(f)_k = \frac{\sigma}{\Delta\theta^2} \cdot (a_k f_{k-1} - b_k f_k + c_k f_{k+1})$
  **end for**
  $f \mathrel{+}= \Delta t \cdot Q_N(f)$
  Return $f$
**end procedure**

### 4.1.3 Adaptative time step for the collision

One of the difficulties in computing an approximate solution to (3.3) is coping with the associated CFL condition (4.13). Indeed, the existence of a locally high $|j(f)|$ greatly decreases the right-hand side of (4.13), which penalizes the whole algorithm. Hence using a global CFL condition for the transport part and the collision part can lead to extremely long computation time.

We propose to decouple the time steps for the transport part and the collision equation at each time step, by using an adaptative method for the latter. Technically, we use the maximal time step associated with the CFL condition to solve the transport part (4.3), $\Delta t = \Delta x$, which incidentally has the advantage of minmizing numerical diffusion. Then, for each $(x_i, y_j)$, we consider (4.4) as a differential equation with final time $\Delta t$, which we solve by using the method described in Section 4.1 with a variable time step $\delta t$ that needs to be recomputed at each time $0 \leq t' \leq \Delta t$:

$$\delta t(t') := \min\left(\frac{\Delta\theta^2}{2\sigma}\exp\left(\mu(f)\frac{-2\sin(\frac{\Delta\theta}{4})}{\sigma}\right), \Delta t - t'\right).$$

This method also works for a constant relaxation $\mu(f) = \mu_0$, and can be preferred because it minimizes the numerical diffusion in the transport equation. Particularly when the constant $\sigma = \frac{\mu}{D}$ is large, in which case the collision CFL (4.14) is much smaller than the transport CFL (4.15).

A comparison between the errors done by the standard and adaptative schemes, respectively, is shown in Figure 5.

## 4.2 Numerical scheme for the transport operator

We use an upwind finite-difference method to solve the transport equation (4.3). We fix $M > 0$ and consider a uniform discretization of the interval $[0, L)$ in $M$ points with $x_i = i\Delta x$, $y_j = j\Delta y$, and $\Delta x = \Delta y = \frac{L}{M}$. To discretize the kinetic equation, we use:

$$\cos\theta\,\partial_x f = \begin{cases} \cos\theta\,\frac{f(x_i) - f(x_{i-1})}{\Delta x} + \mathcal{O}(\Delta x), & \text{if } \cos\theta \geq 0 \\ \cos\theta\,\frac{f(x_i) - f(x_{k+1})}{\Delta x} + \mathcal{O}(\Delta x), & \text{if } \cos\theta \leq 0, \end{cases}$$

and similarly for $\sin(\theta)\partial_y f$. Using this discretization, the standard Euler scheme gives as CFL condition:

$$c\frac{\Delta t}{\Delta x} < 1 \tag{4.15}$$

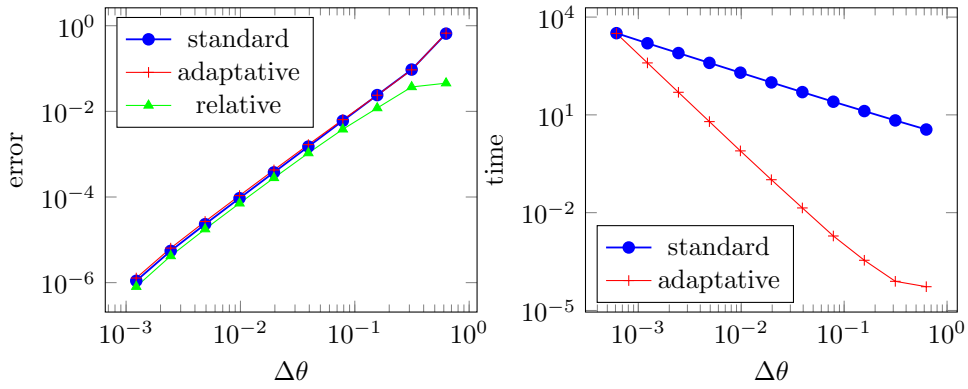


(a) Error in the standard and adaptative model. The *standard* and *adaptative* curves show the maximum of the difference between the computed distribution and the one with lowest $\Delta\theta$. The "relative" curve shows the maximum of the difference between the standard and adaptative solution.

(b) Comparison of the time (in seconds) needed to compute the solution

Figure 5: Comparison of the standard and adaptative methods for the collision operator (Vicsek). Parameters are: $\mu = 1.0$, $\sigma = 0.2$, $\rho = 1.0$, $\Delta t = 8.458 \cdot 10^{-7}$ (standard), $\Delta t = 0.1$ (adaptative), $T = 1.0$. The initial condition is $f_0(\theta) = \rho\left(1 + \frac{1}{5}\sum_{k=1}^{5}\cos(p_k\theta)\right)$ where $p_1 = 1$ and $p_k$ is the prime following $p_{k-1}$.

**Algorithm 2** Transport part eq. (4.3)

**procedure** TRANSPORT($f(x_i, y_j, \theta_k), \Delta t$)
  **for** $i, j, k$ **do**
    $F_{i+\frac{1}{2},j,k} = \begin{cases} c\cos\theta_{i+\frac{1}{2}} f_{i,j,k} & \text{if } \cos\theta_{i+\frac{1}{2}} \le 0 \\ c\cos\theta_{i+\frac{1}{2}} f_{i+1,j,k} & \text{if } \cos\theta_{i+\frac{1}{2}} \ge 0 \end{cases}$
  **end for**
  **for** $i, j, k$ **do**
    $f_{i,j,k}$ += $-\frac{\Delta t}{\Delta x} \cdot (F_{i+\frac{1}{2},j,k} - F_{i-\frac{1}{2},j,k})$
  **end for**
  **for** $i, j, k$ **do**
    $F_{i,j+\frac{1}{2},k} = \begin{cases} c\sin\theta_{j+\frac{1}{2}} f_{i,j,k} & \text{if } \sin\theta_{i+\frac{1}{2}} \le 0 \\ c\sin\theta_{j+\frac{1}{2}} f_{i,j+1,k} & \text{if } \sin\theta_{i+\frac{1}{2}} \ge 0 \end{cases}$
  **end for**
  **for** $i, j, k$ **do**
    $f_{i,j,k}$ += $-\frac{\Delta t}{\Delta y} \cdot (F_{i,j+\frac{1}{2},k} - F_{i,j-\frac{1}{2},k})$
  **end for**
  Return $f$
**end procedure**

## 4.3 Summary

The full algorithm is finally a splitting between the transport and collision part. Notice that the time step $\Delta t$ should satisfy both CFL conditions (4.13) and (4.15). In general, the collisional CFL (4.13) is more restrictive. Therefore, the transport equation will be solved with a small CFL corresponding to large numerical viscosity. Since we aim at studying the large time behavior of the dynamics, this numerical viscosity might drastically change the outcome. Thus, we propose to use an adaptive method for the collisional operator. The idea is to simply iterative $K$ 'small' steps $\delta t = \Delta t/K$ to update the collision part choosing $K$ such that '$\delta t$ satisfies the CFL condition (4.14).

**Algorithm 3** Collision part eq. (4.4)

**procedure** CollisionAdapt($f(\theta_k), \Delta t$)
  Find $K$ such that $\delta t = \Delta t/K$ satisfies (4.14)
  **for** $s$ in $1 : K$ **do**
    $f =$ **Collision**$(f, \delta t)$
  **end for**
  Return $f$
**end procedure**

**Algorithm 4** Full kinetic eq. (3.1)

Fix $\Delta t < \min(\Delta x, \Delta y)/c$
$t = 0$
**while** $t < T$ **do**
  $f^* =$ **Transport**$(f^n, \Delta t)$
  **for** $i, j$ **do**
    $f^{n+1}_{i,j,k} =$ **CollisionAdapt**$(f^*_{i,j,k}, \Delta t)$
  **end for**
  $t \mathrel{+}= \Delta t$
**end while**
Return $f$

# 5 Numerical experiments

## 5.1 Homogeneous case

To first investigate our numerical scheme, we study the homogeneous equation, thus solving only the collision operator (4.4). We present numerical experiment the Vicsek model (3.1), however results are similar with the Frouvelle-Liu dynamics except that the time step $\Delta t$ may have to be adapted since the CFL condition depends on $|\mathbf{j}|$ which varies over time.

As a first sanity check, we estimate the accuracy of the scheme. With this aim, we fix a final time $T = 1$ and time step $\Delta t = .001$. Then, we vary the meshgrid in $\theta$, taking $\Delta\theta \in \{\frac{2\pi}{8}, \frac{2\pi}{16}, \dots, \frac{2\pi}{128}\}$ and estimate the $L^2$ error with the reference solution $f_{ref}$ computing with $\Delta\theta = \frac{2\pi}{256}$. For the initial condition, we use a smooth initial condition:

$$f_0(\theta) = (1.1 + \cos 4\theta) \cdot \exp\left(-\cos\left(\pi(s + s^8)\right)\right), \qquad \text{with } s = \theta/2\pi. \tag{5.1}$$

We use a rather complicated expression to make sure that $f_0$ is non-symmetric. When $f_0$ is symmetric, the mean direction $\bar{\theta}$ is preserved over time, thus the Vicsek dynamics (3.4) becomes a linear evolution equation. Twisting the initial condition $f_0$ guarantees to have a fully non-linear equation.

In figure 6-left, we plot the initial condition $f_0$ along with the reference solution $f_{ref}$ at $t = 1$. The $L^2$ error for various discretization is given in log scale in figure 6-right. We observe that the error is decaying quadratically as expected.

Moreover, we also investigate the large-time behavior of the solution. First, we measure the evolution free entropy $\mathcal{F}$ over time and we observe that it is strictly decreasing (fig. 7-left). Second, we estimate the rate of convergence of $f(t)$ toward an equilibrium distribution. Using semi-log scale in fig. 7-right, we observe a linear decay indicating that the convergence is exponential.

## 5.2 Band formation

In the Vicsek model (3.1), we did not observe the formation of any bands. Rather, the dynamics always converge to a robust global alignment dynamics, where the spatial distribution (first moment of $f$) converges to a constant. The typical long-time behaviour is represented in Figure 8. We postulate that the long-time behaviour of this equation is just to converge to a uniform distribution of Von Mises equilibria to the homogeneous equation.

On the other hand, the Frouvelle-Liu model (3.3) of interaction leads to the observation of bands. Typically, for a fixed set of parameters, we observed two different scenarios regarding the behavior of the local density $\rho$ and mean value $\rho$

$$\rho(t,\mathbf{x}) = \int_{\mathbb{S}^1} f(t,\mathbf{x},\omega)\mathrm{d}\omega \quad , \qquad \bar{\rho} = \frac{\int_{[0,L]^2\times\mathbb{S}^1} f(\mathbf{x},\omega)\mathrm{d}\mathbf{x}\mathrm{d}\omega}{2\pi L^2}, \tag{5.2}$$

For a fixed mean value $\rho$, when the strength of interaction $\mu$ is small compared to the diffusion parameter $\sigma$ (i.e. $\mu \gg \sigma$), we observe that the solution converges to a uniform steady state. However, when $\mu \ll \sigma$, we observe the formation of bands as shown in Figure 9 (in which the x-axis has been reversed to provide better aesthetics). Thus, we retrieve an equivalent of the phase transition dynamics noticed by Frouvelle and Liu in [14]. Those bands were first noticed starting from a random initial condition (Figure 9a). Even though they literally emerge from chaos, they appear to be only meta-stable, as their small inhomogeneity in the direction perpendicular to the propagation amplifies slowly by attracting the neighbour particles and finally lead to high and localized concentrations as shown in Figure 9b. At this point the computation is difficult to continue due to the extremely high computation times required by the CFL condition. Starting from an initial condition which is homogeneous in one direction (e.g. in $y$), however, the observed bands are very stable in time and can be kept alive for apparently an arbitrarily long time (the homogeneity being preserved by our scheme). Such a band is represented in Figure 9c. The initial condition we used is the following:

$$f_0(x,y,\theta) = \bar{\rho}\left(1 + \frac{1}{10}\sum_{k=1}^{5}\cos(p_k\theta) + \cos\left(2p_k\pi\frac{x}{L}\right)\right).$$

Bands were also observed in a modified model which we encoded to take advantage of the preservation of homogeneity in one direction. A resulting band is presented in Figure 9d.

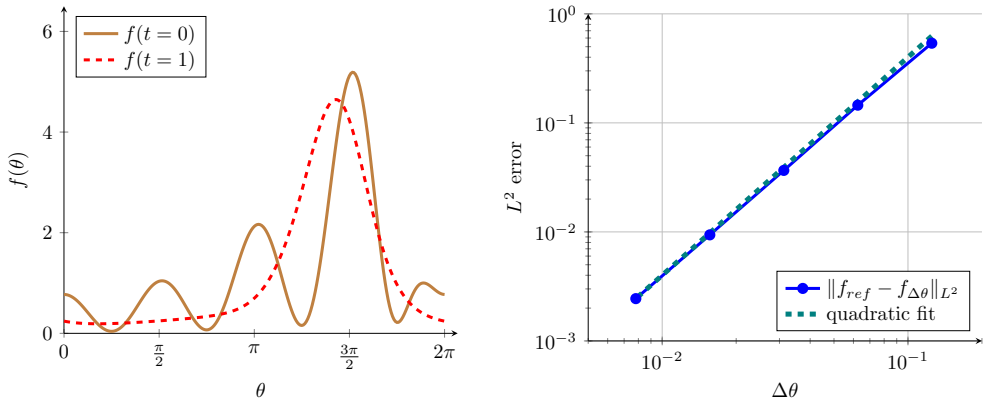


Figure 6: **Left:** the initial condition $f_0$ (5.1) and the reference solution $f_{ref}$ (dashed) computed after $t = 1$ (with $\Delta t = 10^{-3}$ and $\Delta\theta = \frac{2\pi}{256}$). **Right:** $L^2$ error in log scale between the solution $f_{\Delta\theta}$ with the reference solution $f_*$ at $t = 1$. We observe a quadratic accuracy.

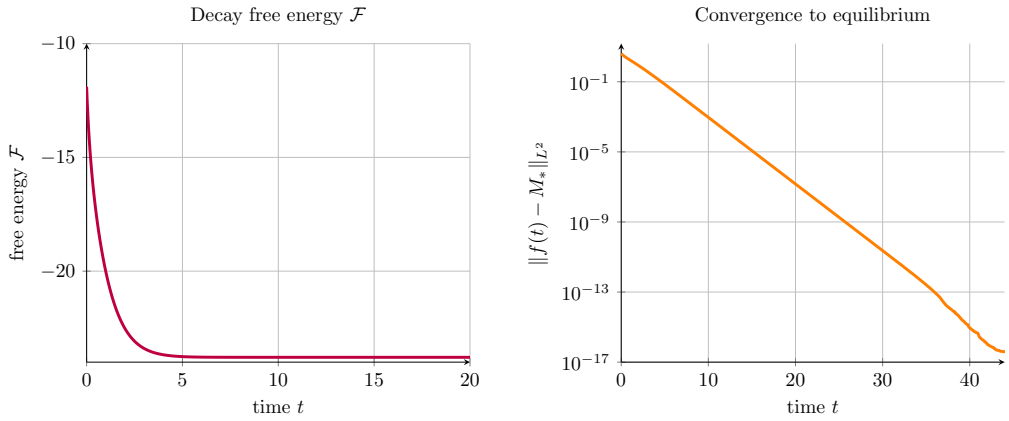


Figure 7: **Left:** evolution of the free energy $\mathcal{F}$ (3.13) over time. The function is strictly decreasing. **Right:** $L^2$ error between the solution $f(t)$ and its equilibrium distribution $M_*$. Since it uses semi-log scale, the convergence is actually exponential.

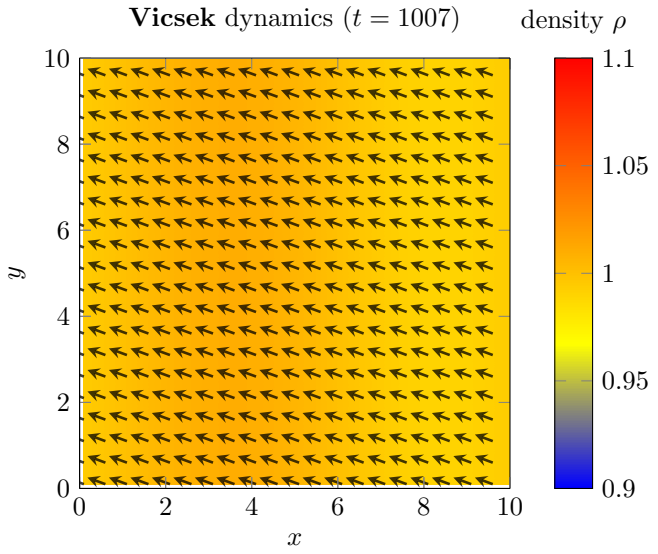


Figure 8: Typical shape of the long-time solution observed in the case of the Vicsek interaction model (obtained starting from a random initial condition) at $t = 1000$. Parameters are: $\mu = 1.0$, $D = 0.2$, $c = 1.0$, $L = 10.0$, $\Delta x = \Delta y = 0.1$, $\Delta\theta = \frac{2\pi}{30}$

Numerical evidences show that the bands cannot be understood as traveling wave solutions to the kinetic equation (3.1), as one may believe at first sight. Indeed, there remains an inner motion inside the bands, that we can reveal by monitoring the maximal value of $\rho$ through time (see Figure 10). This reveals an asymptotically periodic behaviour that strongly resembles the notion of pulsating fronts, which has been extensively studied in the context of reaction-diffusion phenomena [23]. A deeper analytical understanding of this phenomenon is left for future work.

Finally, to strengthen the link between the phase transition and the formation of bands, we show in Figure 11 two kinds of entropy computed for a range of values of the diffusion coefficient $d$ and the mean value of the initial condition $\bar{\rho}$. Figure 11a represents the entropy of $f$ computed against the uniform distribution of the same mass:

$$\mathcal{E}_u[f] = \int_0^L \int_0^L \int_0^{2\pi} f(t, \mathbf{x}, \theta) \log\left(\frac{f(t, \mathbf{x}, \theta)}{\bar{\rho}}\right) \mathrm{d}\theta \mathrm{d}\mathbf{x}.$$

Figure 11b represents the generalized entropy of $f$ computed against the corresponding Von Mises distribution:

$$\mathcal{E}_{VM}[f] = \int_0^L \int_0^L \int_0^{2\pi} f(t, \mathbf{x}, \theta) \log\left(\frac{f(t, \mathbf{x}, \theta)}{M[\bar{\rho}](\theta)}\right) \mathrm{d}\theta \mathrm{d}\mathbf{x},$$

where $M[\bar{\rho}](\theta) = 2\pi\bar{\rho}\frac{\exp\left(\frac{\mu\kappa}{d}\cos(\theta)\right)}{\int_0^{2\pi}\exp\left(\frac{\mu\kappa}{d}\cos(\theta)\right)\mathrm{d}\theta}$ is the only candidate as stationary Von Mises distribution, $\kappa$ satisfying the compatibility condition

$$2\pi\bar{\rho}\frac{\int_0^{2\pi}\cos\theta\exp\left(\frac{\mu\kappa}{d}\cos(\theta)\right)\mathrm{d}\theta}{\int_0^{2\pi}\exp\left(\frac{\mu\kappa}{d}\cos(\theta)\right)\mathrm{d}\theta} = \kappa. \tag{5.3}$$

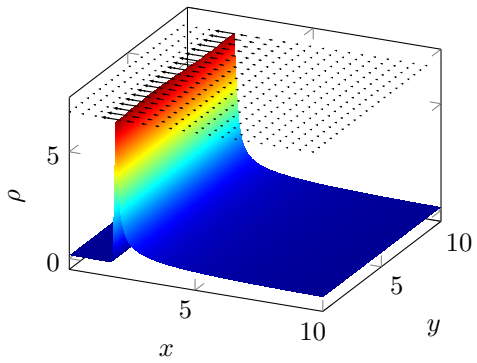


(a) Starting from a random initial condition $t = 1000.0$ ($\bar{\rho} \approx 0.0766$).

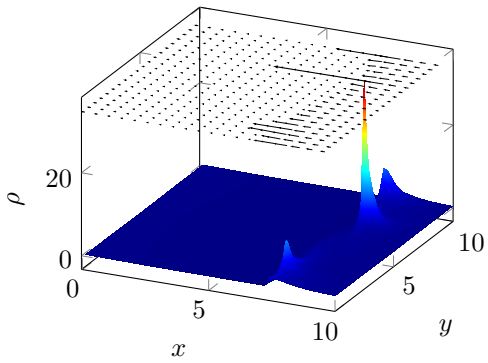


(b) Starting from a random initial condition $t = 1227.0$.

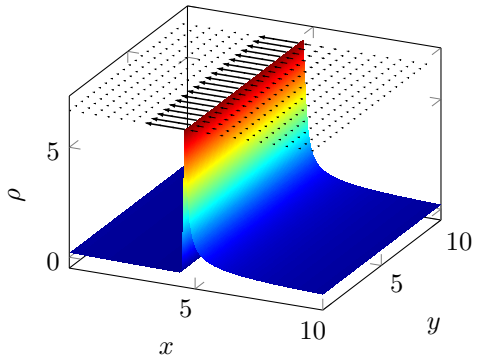


(c) Starting from a homogeneous initial condition, $t = 1007.0$ ($\bar{\rho} = 0.0763$).

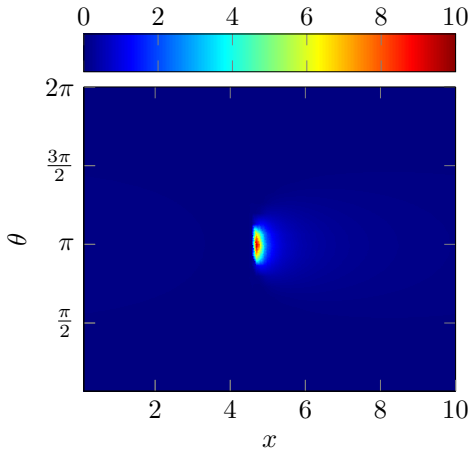


(d) Pseudo-1D code, $t = 1005.0$ ($\bar{\rho} = 0.0763$). Here the real value of $f$ is represented as a function of $x$ and $\theta$.

Figure 9: Different observations of bands. The surface plot corresponds to the observed density $\rho = \int_{\mathbb{S}^1} f(t, \mathbf{x}, \omega) \mathrm{d}\omega$. The arrows on the top correspond to the local mean direction $j(\mathbf{x})$. Figures 9a and 9b were obtained starting from the same random initial condition. Figure 9c was obtained starting from a homgeneous in $y$ initial condition. Figure 9d was obtained by a one-dimensional version of the code. In all cases, the same set of parameters was used: $\mu = 1.0$, $\sigma = 0.2$, $c = 1.0$, $L = 10.0$, $\Delta x = \Delta y = 0.1$, $\Delta\theta = \frac{2\pi}{30}$.

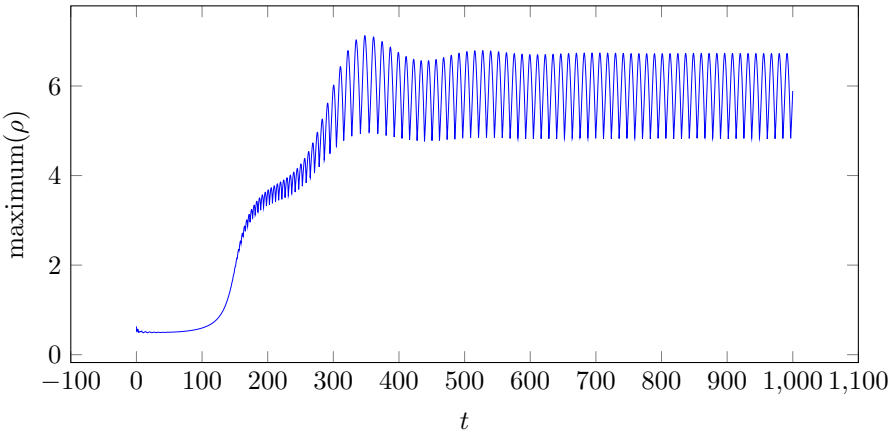


Figure 10: Maximal value of $\rho(t, \mathbf{x})$ as a function of $t$.

Let us recall that the latter has only one solution $\kappa = 0$ when $\sigma \geq \pi\mu\bar{\rho}$, and has exactly one positive solution when $\sigma < \pi\mu\bar{\rho}$ [14].

The match between the two plots suggests that the latter stationary state candidate is never stable except when $\kappa = 0$. Indeed for $\sigma \geq \pi\mu\bar{\rho}$, the uniform distribution is stable for the homogeneous problem and $\kappa = 0$; this corresponds to the top-left part of figure 11a, which suggests that this stability is transferred to the inhomogeneous problem 3.3. For $\sigma < \pi\mu\bar{\rho}$, however, we have $\kappa > 0$ and the stable state for the homogeneous problem is described by the corresponding Von Mises distribution $M[\bar{\rho}](\theta)$; Figure 11b suggests that the inhomogeneous problem behaves otherwise, neither the uniform nor the homogeneous Von Mises distribution corresponding to the long-time behaviour of the equation, except possibly in a very small area near $\sigma \approx \pi\mu\bar{\rho}$ (which appears more clearly in the log-plots 11c and 11d). Instead, the unstability of both homogeneous stationary states could be at the origin of the formation of bands.

# References

[1] M. Aldana and C. Huepe. Phase Transitions in Self-Driven Many-Particle Systems and Related Non-Equilibrium Models: A Network Approach. *Journal of Statistical Physics*, 112(1):135–153, 2003.

[2] F. Bolley, J. Cañizo, and J. Carrillo. Mean-field limit for the stochastic Vicsek model. *Applied Mathematics Letters*, 25(3):339–343, 2012.

[3] S. Camazine, J. L Deneubourg, N. R Franks, J. Sneyd, G. Theraulaz, and E. Bonabeau. Self-organization in biological systems. *Princeton University Press; Princeton, NJ: 2001*, 2001.

[4] J. Carrillo, A. Chertock, and Y. Huang. A finite-volume method for nonlinear nonlocal equations with a gradient flow structure. *Communications in Computational Physics*, 17(01):233–258, 2015.

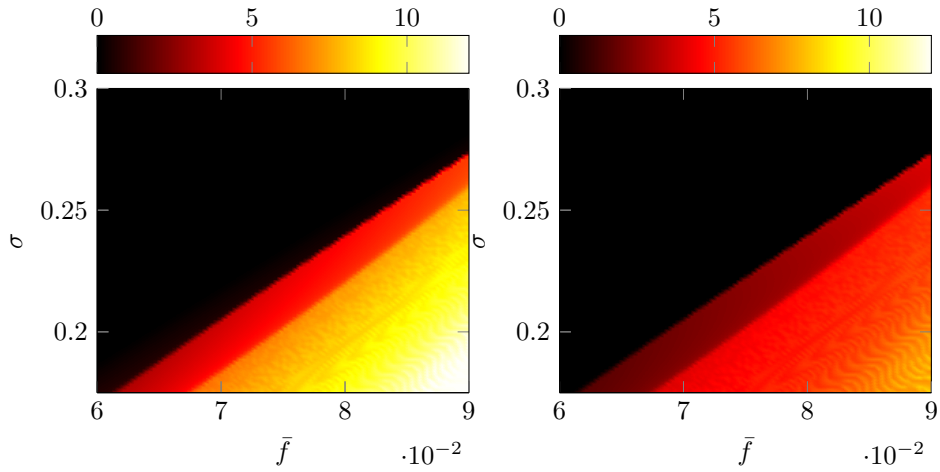


(a) Entropy against the uniform distribution

(b) Entropy against the Von Mises distribution

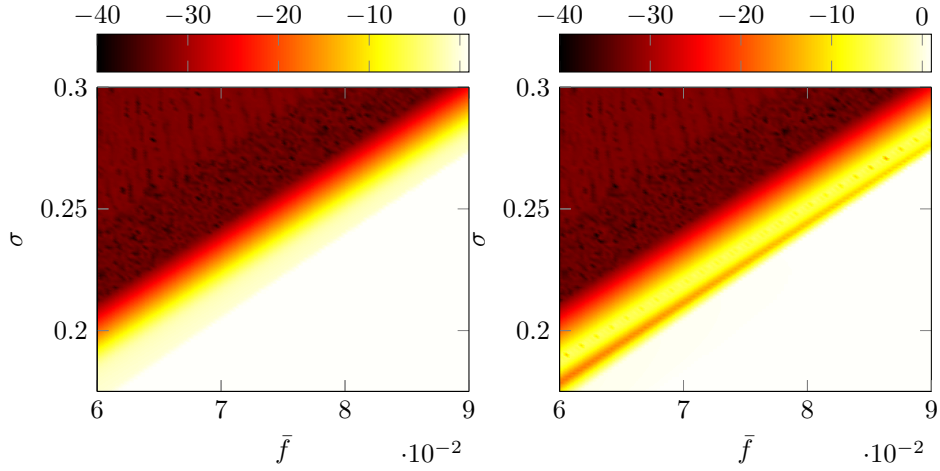


(c) Log-entropy against the uniform distribution

(d) Log-entropy against the Von Mises distribution

Figure 11: Entropies as a function of $\bar{\rho}$ and $\sigma$.

[5] Hugues Chaté, Francesco Ginelli, and Guillaume Grégoire. Comment on "phase transitions in systems of self-propelled agents and related network models". *Physical review letters*, 99(22):229601, 2007.

[6] Hugues Chaté, Francesco Ginelli, Guillaume Grégoire, Fernando Peruani, and Franck Raynaud. Modeling collective motion: variations on the Vicsek model. *The European Physical Journal B*, 64(3-4):451–456, 2008.

[7] P. Degond, A. Frouvelle, and J-G. Liu. Macroscopic limits and phase transition in a system of self-propelled particles. *Journal of nonlinear science*, 23(3):427–456, 2013.

[8] P. Degond, A. Frouvelle, and J-G. Liu. Phase transitions, hysteresis, and hyperbolicity for self-organized alignment dynamics. *Archive for Rational Mechanics and Analysis*, 216(1):63–115, 2015.

[9] P. Degond, J-G. Liu, S. Motsch, and V. Panferov. Hydrodynamic models of self-organized dynamics: derivation and existence theory. *Methods and Applications of Analysis*, 20(2):89–114, 2013.

[10] P. Degond and S. Motsch. Continuum limit of self-driven particles with orientation interaction. *Mathematical Models and Methods in Applied Sciences*, 18(1):1193–1215, 2008.

[11] G. Dimarco and S. Motsch. Self-alignment driven by jump processes: Macroscopic limit and numerical investigation. *Mathematical Models and Methods in Applied Sciences*, 26(07):1385–1410, 2016.

[12] A. Figalli, M-J. Kang, and J. Morales. Global well-posedness of the spatially homogeneous Kolmogorov–Vicsek model as a gradient flow. *Archive for Rational Mechanics and Analysis*, 227(3):869–896, 2018.

[13] Francis Filbet and Chi-Wang Shu. Discontinuous-galerkin methods for a kinetic model of self-organized dynamics. *arXiv preprint arXiv:1705.08129*, 2017.

[14] A. Frouvelle and J-G. Liu. Dynamics in a kinetic model of oriented particles with phase transition. *SIAM Journal on Mathematical Analysis*, 44(2):791–826, 2012.

[15] I. Gamba, J. Haack, and S. Motsch. Spectral method for a kinetic swarming model. *Journal of Computational Physics*, 297:32–46, 2015.

[16] I. Gamba and M-J. Kang. Global weak solutions for Kolmogorov–Vicsek type equations with orientational interactions. *Archive for Rational Mechanics and Analysis*, 222(1):317–342, 2016.

[17] S. Gottlieb, C-W. Shu, and E. Tadmor. Strong stability-preserving high-order time discretization methods. *SIAM review*, 43(1):89–112, 2001.

[18] Guillaume Grégoire and Hugues Chaté. Onset of collective and cohesive motion. *Physical review letters*, 92(2):025702, 2004.

[19] Máté Nagy, István Daruka, and Tamás Vicsek. New aspects of the continuous phase transition in the scalar noise model (SNM) of collective motion. *Physica A: Statistical Mechanics and its Applications*, 373:445–454, 2007.

[20] Karl Oelschläger. A law of large numbers for moderately interacting diffusion processes. *Zeitschrift für Wahrscheinlichkeitstheorie und verwandte Gebiete*, 69(2):279–322, 1985.

[21] T. Vicsek, A. Czirók, E. Ben-Jacob, I. Cohen, and O. Shochet. Novel type of phase transition in a system of self-driven particles. *Physical Review Letters*, 75(6):1226–1229, 1995.

[22] T. Vicsek and A. Zafeiris. Collective motion. *Physics Reports*, 517(3):71–140, 2012.

[23] Jack Xin. Front propagation in heterogeneous media. *SIAM review*, 42(2):161–230, 2000.